Massless Dirac fermions in III-V semiconductor quantum wells

S. S. Krishtopenko,[1,2,*] W. Desrat,[1,*] K. E. Spirin,[2] C. Consejo,[1] S. Ruffenach,[1] F. Gonzalez-Posada,[3] B. Jouault,[1] W. Knap,[1] K. V. Maremyanin,[2] V. I. Gavrilenko,[2] G. Boissier,[3] J. Torres,[3] M. Zaknoune,[4] E. Tournié,[3] and F. Teppe[1,†]

[1]*Laboratoire Charles Coulomb, Université de Montpellier, Centre National de la Recherche Scientifique, F-34095 Montpellier, France*
[2]*Institute for Physics of Microstructures RAS, GSP-105, Nizhni Novgorod 603950, Russia*
[3]*Institut d'Electronique et des Systèmes, Université de Montpellier, Centre National de la Recherche Scientifique, F-34000 Montpellier, France*
[4]*Institut d'Electronique, de Microélectronique et de Nanotechnologie, Lille University, Avenue Poincaré, B.P. 60069, F-59652 Villeneuve d'Ascq, France*

We report on the clear evidence of massless Dirac fermions in two-dimensional system based on III-V semiconductors. Using a gated Hall bar made on a three-layer InAs/GaSb/InAs quantum well, we restore the Landau level fan chart by magnetotransport and unequivocally demonstrate a gapless state in our sample. Measurements of cyclotron resonance at different electron concentrations directly indicate a linear band crossing at the Γ point of the Brillouin zone. Analysis of experimental data within an analytical Dirac-like Hamiltonian allows us not only to determine the velocity ($v_F = 1.8 \times 10^5$ m/s) of massless Dirac fermions, but also to demonstrate a significant nonlinear dispersion at high energies.

Since a relativistic Dirac-like character of charge carriers was demonstrated in monolayer graphene [1], two-dimensional (2D) massless Dirac fermions (DFs) have been intensively studied in condensed matter physics. There are several systems [2], from graphenelike 2D materials (silicene, germanene, etc.) or high-temperature d-wave superconductors to the surfaces of three-dimensional (3D) topological insulators, in which the presence of 2D massless DFs was revealed. Their universal features, such as suppressed backscattering [3], Klein tunneling [4], giant magnetoresistance [5], or their specific response to impurities and magnetic field [6] hold great promises for new nanoscale electronic devices.

Among quantum well (QW) systems, a single-valley spin-degenerate Dirac cone at the Γ point of the Brillouin zone was theoretically predicted [7,8] and experimentally observed [9–12] in HgTe/CdTe QWs. At a critical width, the band gap in these QWs vanishes and the band structure changes from trivial to inverted. The key advantage of QWs over other systems is based on the ability to adjust the DF velocity by adjusting the strain and thickness of the layers. It allows one to vary the ratio between the kinetic energy and Coulomb interaction, which results in a rich variety of phenomena involving massless DFs [13]. However, the massless DFs in HgTe QWs appear only at a fixed temperature, since the temperature changes open a band gap, resulting in a nonzero rest mass of the particles [14–18].

In the search for 2D massless DFs in other QWs, some authors considered theoretically very thin (few atomic layers) conventional III-V semiconductor heterostructures, such as GaN/InN/GaN [19] and GaAs/Ge/GaAs QWs [20]. Depending on the number of atomic layers in these QWs, the band structure can be trivial, inverted, or gapless, just as in HgTe QWs [7,8]. Although considerable progress was made in the fabrication of GaN/InN/GaN and GaAs/Ge/GaAs structures, experimental results confirming the presence of massless DFs in these structures are lacking.

Alternative III-V semiconductor QWs, in which massless DFs have been theoretically predicted, are symmetric three-layer InAs/Ga$_x$In$_{1-x}$Sb/InAs QWs confined between wide-gap AlSb barriers [21]. Depending on their layer thicknesses, these QWs host trivial, quantum spin Hall insulator and gapless states. However, in contrast to the HgTe QWs, the three-layer QWs have a temperature-insensitive band gap, as it has been recently shown by terahertz spectroscopy [22]. Another difference in massless DFs in InAs/Ga$_x$In$_{1-x}$Sb/InAs QWs is the recently predicted [21] large tunability of the quasiparticle's velocity, which can be varied from 1×10^5 to 7×10^5 m/s depending on x and the layer thicknesses. The latter offers the possibility not only to tune the electronic properties [3,4,6] of the DFs, but also to achieve specific nontrivial states induced by electron-electron interactions [23–26].

In this Rapid Communication, we report striking evidence of the presence of massless Dirac fermions in InAs/GaSb/InAs QWs embedded between AlSb barriers. Measuring the magnetoresistance of a gated Hall bar, we restore the Landau level (LL) fan chart in our sample, as first performed by Büttner *et al.* [9] in HgTe QWs. Our experimental data clearly evidence a gapless state. We also measure cyclotron resonance (CR) at different electron concentrations varied by bipolar persistent photoconductivity (PPC) inherent to InAs-based QWs [27–34]. The latter acts as an optical gating and allows one to change the electron concentration in the QW several times. By analyzing the dependence of the cyclotron mass as a function of the concentration, the massless DF velocity is deduced. To analyze these data, we use both realistic band-structure calculations based on an eight-band Kane
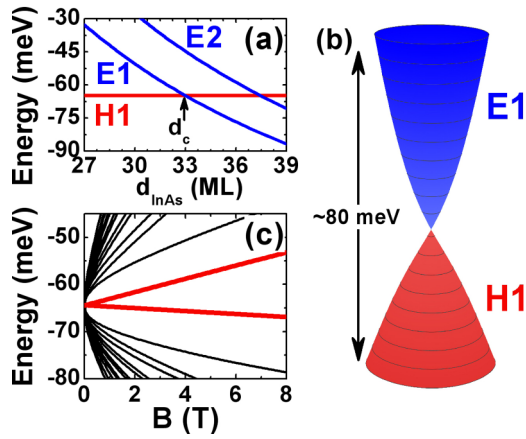
FIG. 1. (a) Subband energies at zero quasimomentum **k** in symmetric InAs/GaSb/InAs QWs as a function of InAs layer thickness d_{InAs}. Blue and red curves correspond to the electronlike and holelike states, respectively. The thickness of the GaSb layer d_{GaSb} equals 12 monolayers (ML). Here, 1 ML corresponds to half of the lattice constant of the bulk material. The zero energy is referenced to the valence-band edge of bulk GaSb. (b) A 3D plot of the Dirac cone describing the energy spectrum at $\mathbf{k} < 0.2$ nm^{-1} for $d_{InAs} = 33$ ML and $d_{GaSb} = 12$ ML. (c) LL fan chart for the gapless state. A pair of zero-mode LLs is presented by the red curves. All the calculations are based on an eight-band Kane model [21].

model [21] and an analytical approach involving a simplified Dirac-like Hamiltonian [8].

As mentioned above, the band structure of three-layer InAs/GaSb/InAs QWs, related to the mutual position of electronlike and holelike subbands, strongly depends on the layer thicknesses [21]. When the InAs and GaSb layers are both thin, the first electronlike ($E1$) and holelike ($H1$) subbands correspond to the conduction and valence bands, respectively, and the QW has a trivial band ordering. For thicker layers, the $E1$ subband drops below the $H1$ subband, as shown in Fig. 1(a), and the system has an inverted band ordering. In this case, the conduction and valence bands are represented by holelike and electronlike levels, respectively.

One can use a simplified Dirac-like Hamiltonian [8] to describe the electronic states when the energy difference between the $E1$ and $H1$ subbands is small. Within the representation defined by the basis $|E1, +\rangle$, $|H1, +\rangle$, $|E1, -\rangle$, $|H1, -\rangle$, it has the form

$$H(\mathbf{k}) = \begin{pmatrix} H_D(\mathbf{k}) & 0 \\ 0 & H_D^*(-\mathbf{k}) \end{pmatrix},$$

$$H_D(\mathbf{k}) = \epsilon(\mathbf{k}) + \sum_{i=1}^{3} d_i(\mathbf{k})\sigma_i,$$

where the asterisk stands for complex conjugation, $\mathbf{k} = (k_x, k_y)$ is the momentum in the QW plane, σ_i are the Pauli matrices, $\epsilon_{\mathbf{k}} = C - D(k_x^2 + k_y^2)$, $d_1(\mathbf{k}) = -Ak_x$, $d_2(\mathbf{k}) = -Ak_y$, and $d_3(\mathbf{k}) = M - B(k_x^2 + k_y^2)$. The structure parameters A, B, C, D, M depend on the layer thicknesses. The mass parameter M is positive for a trivial band ordering and negative for an inverted band structure. If we only keep the terms up to linear order in k for each spin, then

$H_D(\mathbf{k})$ and $H_D^*(-\mathbf{k})$ at $M = 0$ correspond to massless Dirac Hamiltonians. We note that the latter is valid if the InAs/GaSb/InAs QW has an inversion symmetry in the growth direction [35]. In this case, the $E1$ and $H1$ subbands cross at the Γ point, and their energy dispersion calculated from an eight-band Kane model is found to linearly depend on the quasimomentum at small **k**, as shown in Fig. 1(b).

Besides the linear terms, $H_D(\mathbf{k})$ also contains quadratic terms, which cannot be neglected even at the energies close to the band crossing point. Moreover, they result in relevant differences between conventional massless DFs in graphene [1,3,4,6] and the ones in symmetric InAs/GaSb/InAs QWs (and in HgTe QWs [9–11] as well). LLs in graphene are characterized by both a square-root dependence of their energies on the magnetic field and the presence of so-called *zero-energy* LLs independent of the field. Note that all LLs in graphene have a spin degeneracy (for simplicity, we consider the electrons in one valley and neglect the small Zeeman effect). This case is described by the linear terms in $H_D(\mathbf{k})$ and $H_D^*(-\mathbf{k})$ at $M = 0$ [36].

The parabolic terms remove the spin degeneracy of all LLs [36] and, particularly, transform the spin-degenerate *zero-energy* LL into a pair of spin-polarized *zero-mode* LLs [37], as shown in Fig. 1(c). The electronlike zero-mode LL splits from the edge of the $E1$ subband and tends toward a high energy with increasing magnetic field. In contrast, the second level, which decreases with magnetic field, has a holelike character and arises from the $H1$ subband. Therefore, the crossing of the zero-mode LLs at a finite value of the magnetic field occurs in the inverted region, $M < 0$, and is absent for $M > 0$ [17]. A crossing of the zero-mode LLs at zero magnetic field gives a direct indication of the massless DFs in the QW.

The sample studied in this work was grown by molecular beam epitaxy (MBE) on a semi-insulating (001) GaAs substrate with a relaxed GaSb buffer. In order to get the gapless state, the thicknesses of InAs and GaSb layers were 33 and 14 ML, respectively (see Fig. 1). After the growth, a 50-μm-wide gated Hall bar was fabricated by using a single-mesa process. All details are provided in the Supplemental Material [36].

First, we investigate magnetotransport in our sample. Figure 2(a) presents the magnetic field dependence of the longitudinal and Hall resistances at $T = 1.7$ K. The Hall density extracted from the measurements is equal to $n_S = 5.1 \times 10^{11}$ cm^{-2} with electron carriers at zero gate voltage V_g and a mobility of $\mu_e = 1.65 \times 10^4$ cm^2 V^{-1} s^{-1}. The Hall resistance shows well-defined plateaus as a function of magnetic field B at both even and odd multiples of h/e^2 associated with the minima in the Shubnikov–de Haas (ShdH) oscillations, proving a 2D character of charge carriers in our structure. To vary the carrier density in the QW, we apply a gate voltage V_g to the top gate. Typical gate voltage dependencies of R_{xx} and R_{xy} at $B = 6.5$ T are shown in Fig. 2(b) (the low-field data are provided in the Supplemental Material [36]).

The longitudinal resistance shows clear oscillations on each side as a function of V_g of the central peak occurring at $V_{DP} \simeq -4$ V when the Hall resistance presents $\pm 0.5\, h/e^2$ plateaus and a sign reversal. These features demonstrate a change of carrier concentration at different V_g and the inversion of the type of carriers from electrons to holes at large negative gate voltages. Furthermore, an insulating behavior
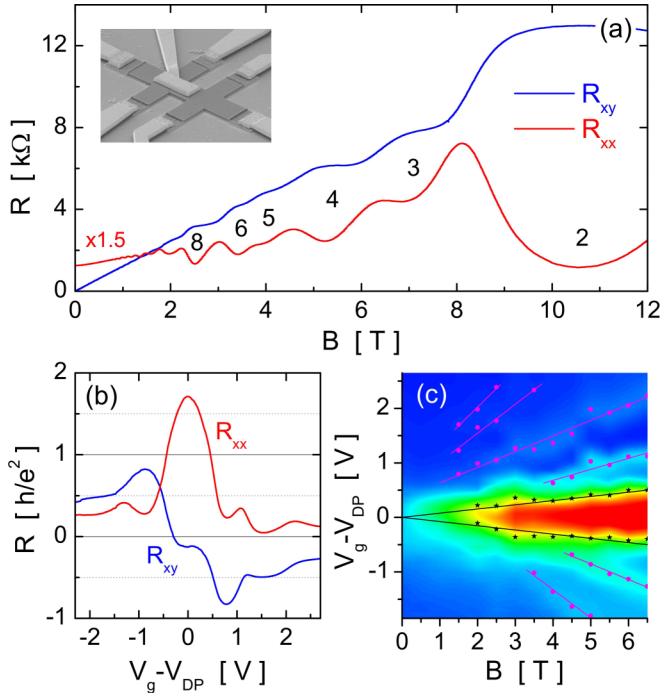
FIG. 2. (a) Longitudinal and Hall resistances as a function of magnetic field at $T = 1.7$ K and $V_g = 0$ V. Electron microscopy image of the Hall bar is shown in the inset. (b) R_{xx} and R_{xy} vs V_g at $T = 1.7$ K and $B = 6.5$ T. (c) Color map of the longitudinal resistance as a function of V_g and B. Black stars indicate h/e^2 values and red dots the peak values of R_{xx}.

is observed at around $V_g = V_{DP}$ with $R_{xx} > h/e^2$ and small values of R_{xy}. The evolution of this insulating state is plotted in a 2D color map of R_{xx} as a function of V_g and B [Fig. 2(c)]. It is evident that the size of the insulating region (red area) increases with B. The linear extrapolation down to zero field of the $R_{xx} = h/e^2$ points (black stars), corresponding to the position of the zero-mode LLs [9,17] and delimiting the high resistance region for $B > 2$ T, demonstrates that the insulating state vanishes at $B = 0$ T. This is also confirmed by the analysis of $d\sigma_{xy}/dV_g$ provided in the Supplemental Material [36]. Thus, the crossing of the zero-mode LLs at $B = 0$ T indeed confirms the gapless state in our sample. Traces of higher LLs of electrons and holes are also seen for $V_g - V_{DP}$ higher than 0.5 V and lower than -0.5 V, respectively.

The hallmark of 2D massless DFs is a specific sequence of quantum Hall plateaus observed at odd multiples of $g_v e^2/h$, where g_v is the valley degeneracy factor [3]. In HgTe QWs ($g_v = 1$), the odd-integer quantum Hall sequence is much less pronounced [9] than in graphene [1] ($g_v = 2$) and is observed at small (less than 1 T) magnetic fields only. The latter is caused by a prominent contribution of the parabolic terms in $H_D(\mathbf{k})$, which remove the spin degeneracy of all LLs already at moderate fields as discussed above. In our sample, both *odd* and *even* plateaus are observed (see Fig. 2), and the quantum Hall effect resembles the one in conventional 2D electron gas [38]. This may be interpreted in two different ways.

First, a large contribution of terms proportional to B and D in $H_D(\mathbf{k})$ results in a significant spin splitting of LLs, making the observation of an odd-integer sequence
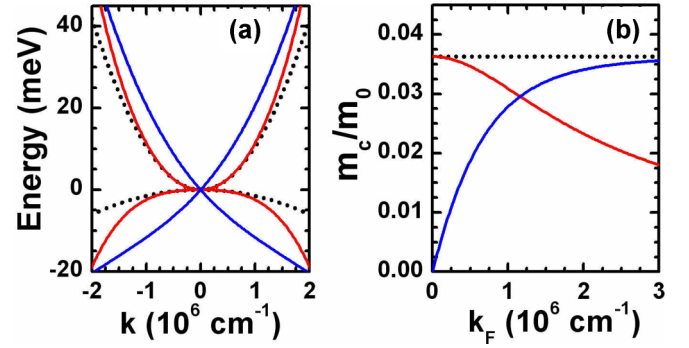
FIG. 3. (a) Band dispersion and (b) cyclotron mass m_c in the conduction band as a function of Fermi momentum, $k_F = \sqrt{2\pi n_S}$ for the gapless states with linear (blue curves) and parabolic band touching at the Γ point. Two cases for parabolic touching, when the conduction and valence bands have the same ($\mathcal{A} = 0$) and opposite ($\mathcal{A} \neq 0$) parity [36], are represented by dotted black and solid red curves, respectively. The following band parameters were used in the calculation: $C = 0$ meV, $A = 150$ meV nm, $\mathcal{A} = 35$ meV nm³, $B = -600$ meV nm², and $D = -450$ meV nm².

impossible. Second, our sample may host the gapless state with parabolic band touching. As shown in the Supplemental Material [36], band dispersion in k for the latter case up to the third order has the form

$$E_{k^2}(k) = C - Dk^2 \pm k^2\sqrt{B^2 + \mathcal{A}^2 k^2}, \qquad (1)$$

where "+" and "−" represent to the conduction and valence bands, respectively. Here, $\mathcal{A} \neq 0$ corresponds to the opposite parity of the conduction and valence band, while for the same parity, one should set $\mathcal{A} = 0$ [36]. Note that the linear dispersion is described by $E_k(k) = C - Dk^2 \pm k\sqrt{A^2 + B^2 k^2}$. The band dispersions at specific parameters are shown in Fig. 3(a).

An efficient way to discriminate these two gapless states is the measurement of quasiclassical CR at different Fermi level positions. Applying a quasiclassical quantization rule to $E_k(k)$ and $E_{k^2}(k)$, the cyclotron mass m_c in the conduction band as a function of Fermi momentum $k_F = \sqrt{2\pi n_S}$ has the forms

$$m_c^{(k)}(k_F) = \frac{\hbar^2 k_F \sqrt{A^2 + B^2 k_F^2}}{A^2 + 2B^2 k_F^2 - 2Dk_F\sqrt{A^2 + B^2 k_F^2}} \qquad (2)$$

and

$$m_c^{(k^2)}(k_F) = \frac{\hbar^2 \sqrt{B^2 + \mathcal{A}^2 k_F^2}}{2B^2 + 3\mathcal{A}^2 k_F^2 - 2D\sqrt{B^2 + \mathcal{A}^2 k_F^2}} \qquad (3)$$

for the linear and parabolic cases, respectively. As seen from Fig. 3(b), the linear and parabolic gapless states show different behaviors of the cyclotron mass as a function of k_F.

Figures 4(a) and 4(b) show CR spectra measured at $T = 4.2$ K with both backward wave oscillators (BWOs) at 845 GHz [39,40] and quantum cascade lasers (QCLs) at 3 THz [41] (pulse duration of 3 μs; repetition period of 100–200 μs) at different electron concentrations varied by using the PPC effect [36]. The measurements were performed on an unprocessed sample with the electron concentration being changed
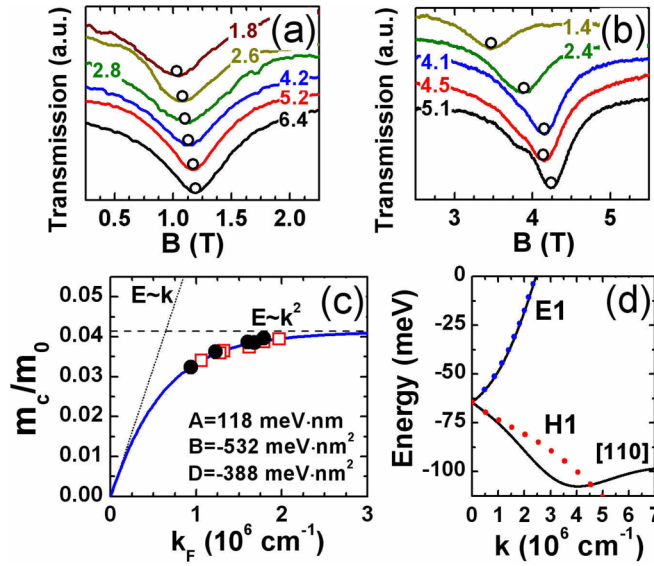
FIG. 4. (a), (b) CR spectra at $T = 4.2$ K of electrons measured with (a) BWO at 845 GHz and (b) QCL at 3 THz for different values of electron concentration. The symbols mark the positions of CR lines. The numbers over the curves show n_S in 10^{11} cm^{-2}. (c) Cyclotron mass m_c as a function of Fermi momentum $k_F = \sqrt{2\pi n_S}$. The open and solid symbols correspond to the values obtained by BWO and QCL, respectively. The bold blue curve is the fitting to Eq. (2). (d) Comparison of band dispersion calculated within the eight-band Kane model with the one described by a simplified Dirac-like Hamiltonian with the parameters shown in (c). Parameter C is chosen to have a coincidence of the band crossing point in two models.

by varying the time illumination from red and blue light-emitting diodes placed close to the sample. The GHz/THz radiation passing through the sample was detected either by a silicon bolometer (for BWO) or Ge:Ga photoresistor (for QCL). The electron concentration was determined along with the CR measurements via magnetotransport measurements in the van der Pauw or two-terminal geometry.

All the spectra contain a single CR line, defining the cyclotron mass m_c at the Fermi level. As seen from Figs. 4(a) and 4(b), CR lines shift toward a high magnetic field with increasing electron concentration. This indicates that the cyclotron mass is strictly an increasing function of n_S. This fact excludes the gapless state with parabolic band touching in our sample. As discussed above, this mass dependence corresponds to the gapless state with linear band crossing. In order to extract the parameters of massless DFs, we have fitted our experimental data by Eq. (2). A good agreement with experimental values is achieved for $A = 118$ meV nm, $B = -532$ meV nm^2, and $D = -388$ meV nm^2. Additionally,

we plot the dependencies for $m_c = \hbar^2 k_F/A$ (dotted curve) and $m_c = \hbar^2/(2|B| - 2D)$ (dashed curve) for pure linear and quadratic band dispersions, respectively.

Figure 4(c) shows that although there are indeed massless DFs with velocity $v_F = A/\hbar = 1.8 \times 10^5$ m/s, they only exist in the immediate vicinity of the Γ point at $n_S \leqslant 10^{10}$ cm^{-2}, while the terms proportional to B and D are relevant at higher concentrations. Note that additional measurements of the temperature dependence of the conductivity at the charge neutrality point also evidence the massless DFs (see the Supplemental Material [36]). The existence of pure massless DFs at small electron concentrations is consistent with the absence of an odd sequence of quantum Hall plateaus in the magnetotransport of our sample. For instance, for an odd Hall plateau with $5e^2/h$ corresponding to a LL filling factor $\nu = 5$ in the linear dispersion regime, one should have well-resolved peaks of R_{xx} at a magnetic field of 0.08 T. The latter cannot be achieved at the electron mobility of our sample.

Figure 4(d) compares the band structure of the sample numerically calculated within the eight-band Kane model with the analytical expression for $E_k(k)$ with the parameters extracted from the fitting $m_c(k_F)$. There is indeed a good agreement for the conduction band, while the valence band is well described at a small quasimomentum only. This is also typical for HgTe/CdTe QWs [16,17], in which the discrepancy for the valence band is explained by the effect of the remote subbands beyond the simplified Dirac-like Hamiltonian $H_D(\mathbf{k})$ [42].

In conclusion, we have clearly observed massless DFs in III-V semiconductor QWs. Magnetotransport experiments on a gated Hall bar allow us to demonstrate the absence of a band gap in our structure. The measurements of CR at different concentrations allow us not only to determine the velocity ($v_F = 1.8 \times 10^5$ m/s) of the massless DFs, but also demonstrate the significant effect of nonlinear dispersion at high energies. Experimental dispersion of the massless DFs is in good agreement with realistic band-structure calculations based on the eight-band Kane Hamiltonian.

[1] K. S. Novoselov, A. K. Geim, S. V. Morozov, D. Jiang, M. I. Katsnelson, I. V. Grigorieva, S. V. Dubonos, and A. A. Firsov, Nature (London) **438**, 197 (2005).

[2] T. O. Wehling, A. M. Black-Schaffer, and A. V. Balatsky, Adv. Phys. **63**, 1 (2014).

[3] A. H. Castro Neto, F. Guinea, N. M. R. Peres, K. S. Novoselov, and A. K. Geim, Rev. Mod. Phys. **81**, 109 (2009).

[4] C. W. J. Beenakker, Rev. Mod. Phys. **80**, 1337 (2008).

[5] T. Liang, Q. Gibson, M. N. Ali, M. Liu, R. J. Cava, and N. P. Ong, Nat. Mater. **14**, 280 (2015).

[6] K. S. Novoselov, A. K. Geim, S. V. Morozov, D. Jiang, Y. Zhang, S. V. Dubonos, I. V. Grigorieva, and A. A. Firsov, Science **306**, 666 (2004).

[7] L. G. Gerchikov and A. V. Subashiev, Phys. Status Solidi B **160**, 443 (1990).

[8] B. A. Bernevig, T. L. Hughes, and S.-C. Zhang, Science **314**, 1757 (2006).

[9] B. Büttner, C. Liu, G. Tkachov, E. Novik, C. Brüne, H. Buhmann, E. Hankiewicz, P. Recher, B. Trauzettel, S. Zhang, and L. Molenkamp, Nat. Phys. **7**, 418 (2011).

[10] M. Zholudev, F. Teppe, M. Orlita, C. Consejo, J. Torres, N. Dyakonova, M. Czapkiewicz, J. Wróbel, G. Grabecki, N. Mikhailov, S. Dvoretskii, A. Ikonnikov, K. Spirin, V. Aleshkin, V. Gavrilenko, and W. Knap, Phys. Rev. B **86**, 205420 (2012).

[11] J. Ludwig, Y. B. Vasilyev, N. N. Mikhailov, J. M. Poumirol, Z. Jiang, O. Vafek, and D. Smirnov, Phys. Rev. B **89**, 241406 (2014).

[12] A. V. Ikonnikov, S. S. Krishtopenko, O. Drachenko, M. Goiran, M. S. Zholudev, V. V. Platonov, Y. B. Kudasov, A. S. Korshunov, D. A. Maslov, I. V. Makarov, O. M. Surdin, A. V. Philippov, M. Marcinkiewicz, S. Ruffenach, F. Teppe, W. Knap, N. N. Mikhailov, S. A. Dvoretsky, and V. I. Gavrilenko, Phys. Rev. B **94**, 155421 (2016).

[13] V. N. Kotov, B. Uchoa, V. M. Pereira, F. Guinea, and A. H. Castro Neto, Rev. Mod. Phys. **84**, 1067 (2012).

[14] S. Wiedmann, A. Jost, C. Thienel, C. Brüne, P. Leubner, H. Buhmann, L. W. Molenkamp, J. C. Maan, and U. Zeitler, Phys. Rev. B **91**, 205311 (2015).

[15] S. S. Krishtopenko, I. Yahniuk, D. B. But, V. I. Gavrilenko, W. Knap, and F. Teppe, Phys. Rev. B **94**, 245402 (2016).

[16] M. Marcinkiewicz, S. Ruffenach, S. S. Krishtopenko, A. M. Kadykov, C. Consejo, D. B. But, W. Desrat, W. Knap, J. Torres, A. V. Ikonnikov, K. E. Spirin, S. V. Morozov, V. I. Gavrilenko, N. N. Mikhailov, S. A. Dvoretskii, and F. Teppe, Phys. Rev. B **96**, 035405 (2017).

[17] A. M. Kadykov, S. S. Krishtopenko, B. Jouault, W. Desrat, W. Knap, S. Ruffenach, C. Consejo, J. Torres, S. V. Morozov, N. N. Mikhailov, S. A. Dvoretskii, and F. Teppe, Phys. Rev. Lett. **120**, 086401 (2018).

[18] F. Teppe, M. Marcinkiewicz, S. S. Krishtopenko, S. Ruffenach, C. Consejo, A. M. Kadykov, W. Desrat, D. But, W. Knap, J. Ludwig, S. Moon, D. Smirnov, M. Orlita, Z. Jiang, S. V. Morozov, V. Gavrilenko, N. N. Mikhailov, and S. A. Dvoretskii, Nat. Commun. **7**, 12576 (2016).

[19] M. S. Miao, Q. Yan, C. G. Van de Walle, W. K. Lou, L. L. Li, and K. Chang, Phys. Rev. Lett. **109**, 186803 (2012).

[20] D. Zhang, W. Lou, M. Miao, S.-C. Zhang, and K. Chang, Phys. Rev. Lett. **111**, 156402 (2013).

[21] S. S. Krishtopenko and F. Teppe, Sci. Adv. **4**, eaap7529 (2018).

[22] S. S. Krishtopenko, S. Ruffenach, F. Gonzalez-Posada, G. Boissier, M. Marcinkiewicz, M. A. Fadeev, A. M. Kadykov, V. V. Rumyantsev, S. V. Morozov, V. I. Gavrilenko, C. Consejo, W. Desrat, B. Jouault, W. Knap, E. Tournié, and F. Teppe, Phys. Rev. B **97**, 245419 (2018).

[23] D. I. Pikulin and T. Hyart, Phys. Rev. Lett. **112**, 176403 (2014).

[24] J. C. Budich, B. Trauzettel, and P. Michetti, Phys. Rev. Lett. **112**, 146405 (2014).

[25] L. Du, X. Li, W. Lou, G. Sullivan, K. Chang, J. Kono, and R.-R. Du, Nat. Commun. **8**, 1971 (2017).

[26] F. Xue and A. H. MacDonald, Phys. Rev. Lett. **120**, 186802 (2018).

[27] C. Gauer, J. Scriba, A. Wixforth, J. P. Kotthaus, C. Nguyen, G. Tuttle, J. H. English, and H. Kroemer, Semicond. Sci. Technol. **8**, S137 (1993).

[28] Y. G. Sadofyev, A. Ramamoorthy, J. P. Bird, S. R. Johnson, and Y.-H. Zhang, Appl. Phys. Lett. **86**, 192109 (2005).

[29] V. Y. Aleshkin, V. I. Gavrilenko, D. M. Gaponova, A. V. Ikonnikov, K. V. Maremyanin, S. V. Morozov, Y. G. Sadofyev, S. R. Johnson, and Y. H. Zhang, Semiconductors **39**, 22 (2005).

[30] V. I. Gavrilenko, A. V. Ikonnikov, S. S. Krishtopenko, A. A. Lastovkin, K. V. Maremyanin, Y. G. Sadofyev, and K. E. Spirin, Semiconductors **44**, 616 (2010).

[31] K. E. Spirin, K. P. Kalinin, S. S. Krishtopenko, K. V. Maremyanin, V. I. Gavrilenko, and Y. G. Sadofyev, Semiconductors **46**, 1396 (2012).

[32] B. Tong, Z. Han, T. Li, C. Zhang, G. Sullivan, and R.-R. Du, AIP Adv. **7**, 075211 (2017).

[33] S. Ruffenach, S. S. Krishtopenko, L. S. Bovkun, A. V. Ikonnikov, M. Marcinkiewicz, C. Consejo, M. Potemski, B. Piot, M. Orlita, B. R. Semyagin, M. A. Putyato, E. A. Emelyanov, V. V. Preobrazhenskii, W. Knap, F. Gonzalez-Posada, G. Boissier, E. Tournié, F. Teppe, and V. I. Gavrilenko, JETP Lett. **106**, 727 (2017).

[34] G. Knebl, P. Pfeffer, S. Schmid, M. Kamp, G. Bastard, E. Batke, L. Worschech, F. Hartmann, and S. Höfling, Phys. Rev. B **98**, 041301 (2018).

[35] S. Murakami, S. Iso, Y. Avishai, M. Onoda, and N. Nagaosa, Phys. Rev. B **76**, 205304 (2007).

[36] See Supplemental Material at http://link.aps.org/supplemental/10.1103/PhysRevB.99.121405 for a brief discussion of the simplified Dirac-like model in magnetic fields, details of magnetotransport measurements, and the spectral studies of persistent photoconductivity of our sample, which contains Refs. [43–51].

[37] M. König, S. Wiedmann, C. Brüne, A. Roth, H. Buhmann, L. W. Molenkamp, X.-L. Qi, and S.-C. Zhang, Science **318**, 766 (2007).

[38] K. v. Klitzing, G. Dorda, and M. Pepper, Phys. Rev. Lett. **45**, 494 (1980).

[39] V. Y. Aleshkin, V. I. Gavrilenko, A. V. Ikonnikov, Y. G. Sadofyev, J. P. Bird, S. R. Johnson, and Y. H. Zhang, Semiconductors **39**, 62 (2005).

[40] K. P. Kalinin, S. S. Krishtopenko, K. V. Maremyanin, K. E. Spirin, V. I. Gavrilenko, A. A. Biryukov, N. V. Baidus, and B. N. Zvonkov, Semiconductors **47**, 1485 (2013).

[41] A. V. Ikonnikov, A. V. Antonov, A. A. Lastovkin, V. I. Gavrilenko, Y. G. Sadof'ev, and N. Samal, Semiconductors **44**, 1467 (2010).

[42] S. S. Krishtopenko and F. Teppe, Phys. Rev. B **97**, 165408 (2018).

[43] I. Semenikhin, A. Zakharova, K. Nilsson, and K. A. Chao, Phys. Rev. B **76**, 035335 (2007).

[44] I. Semenikhin, A. Zakharova, and K. A. Chao, Phys. Rev. B **77**, 113307 (2008).

[45] C. Charpentier, S. Fält, C. Reichl, F. Nichele, A. N. Pal, P. Pietsch, T. Ihn, K. Ensslin, and W. Wegscheider, Appl. Phys. Lett. **103**, 112102 (2013).

[46] K. Bolotin, K. Sikes, Z. Jiang, M. Klima, G. Fudenberg, J. Hone, P. Kim, and H. Stormer, Solid State Commun. **146**, 351 (2008).

[47] G. M. Gusev, D. A. Kozlov, A. D. Levin, Z. D. Kvon, N. N. Mikhailov, and S. A. Dvoretsky, Phys. Rev. B **96**, 045304 (2017).

[48] S. S. Krishtopenko, W. Knap, and F. Teppe, Sci. Rep. **6**, 30755 (2016).

[49] D. G. Rothe, R. W. Reinthaler, C.-X. Liu, L. W. Molenkamp, S.-C. Zhang, and E. M. Hankiewicz, New J. Phys. **12**, 065012 (2010).

[50] G. Tuttle, H. Kroemer, and J. H. English, J. Appl. Phys. **65**, 5239 (1989).

[51] G. Tuttle, H. Kroemer, and J. H. English, J. Appl. Phys. **67**, 3032 (1990).